forests

MDPI

Article

Intra-Crown Microclimatic Heterogeneity and Phenological Buffering: A High-Resolution UAV Study of Flowering and Autumn Leaf Senescence

Min-Kyu Park [1,*], Hun-Gi Choi [2], Yun-Young Kim [2] and Dong-Hak Kim [2]

[1] Independent Researcher, Namyangju 12095, Republic of Korea
[2] Forest Biodiversity Conservation Division, Korea National Arboretum, Pocheon 11186, Republic of Korea; 09gnsrl@korea.kr (H.-G.C.); yuns0809@korea.kr (Y.-Y.K.); ddd9417@korea.kr (D.-H.K.)
* Correspondence: pmkpmk@kakao.com; Tel.: +82-10-2596-2327

Abstract

While climate change shifts plant phenology, conventional satellite-based studies often overlook intra-individual variations due to spatial averaging. This study utilized high-resolution UAV imagery and Digital Surface Models (DSMs) to investigate how intra-crown microclimatic heterogeneity affects the spatiotemporal patterns of flowering and autumn leaf senescence. *Rhododendron yedoense* f. *poukhanense* (H.Lév.) M. Sugim (RY) and *Acer triflorum* Kom. (AT) were monitored at the Korea National Arboretum, with 23 time-series images acquired between April and November 2025. Cumulative solar duration was calculated for 0.5 m intra-crown grids, and phenological events were detected using derivative analysis of vegetation indices (Red Chromatic Coordinate [RCC] and Green Chromatic Coordinate [GCC]). The results confirmed asynchrony in phenological events within single individuals depending on crown sectors. However, the linear relationship between intra-crown microclimatic heterogeneity and phenological duration was statistically weak ($\rho > 0.05$), suggesting that strong physiological buffering mitigates the direct impact of spatial light variation. Despite this buffering, species-specific response patterns were observed: RY exhibited spatially independent flowering responses, whereas AT maintained relatively higher synchrony. Furthermore, AT showed a "Phenological Velocity" gap, where sunlit sectors tended to experience senescence approximately 1.12 days later than shaded areas**, while RY showed no significant directional lag.** This research demonstrates that phenological responses can be spatially dispersed even within an individual, and the buffering mechanisms against environmental variability differ by crown structure and growth form. These findings highlight the necessity of individual-level spatial resolution in understanding plant responses to climate change.

Keywords: bet-hedging; photogrammetry; canopy architecture; phenological plasticity; near-surface remote sensing

Check for updates

Academic Editor: Aleksandar Dj Valjarević

Received: 14 January 2026
Revised: 18 February 2026
Accepted: 25 February 2026
Published: 10 March 2026

Copyright: © 2026 by the authors. Licensee MDPI, Basel, Switzerland. This article is an open access article distributed under the terms and conditions of the Creative Commons Attribution (CC BY) license.

1. Introduction

Climate change is altering plant phenology on a global scale. These changes affect not only the timing of seasonal transitions—such as flowering, leaf unfolding, leaf coloring, and leaf fall—but also have broad impacts on ecosystem functions and interspecific interactions [1,2]. Consequently, quantitatively observing phenological phenomena and understanding their changing mechanisms have become core topics in ecology and climate change research [3,4].

Remote sensing has played a crucial role in phenological research by enabling the systematic analysis of seasonal vegetation variations based on long-term, large-area data [5–7]. Satellite-based studies have significantly contributed to identifying phenological patterns at regional or landscape scales. These studies, utilizing time-series vegetation indices, have successfully revealed long-term trends such as the advancement of spring phenology and the delay of autumn senescence, demonstrating a close correlation between phenological responses and rising temperatures [1,3,8].

However, this approach inevitably involves spatial averaging because the observation unit is limited to the pixel or community level [9]. As a result, differences between individuals of the same species or within the same environmental conditions, as well as subtle phenological variations occurring within a single individual, are likely to be eliminated during the analysis process [10].

Recent advancements in high-resolution Unmanned Aerial Vehicle (UAV) remote sensing technology offer new possibilities to overcome these limitations [11]. Drone orthomosaics provide a spatial resolution of a few centimeters, allowing for the direct observation of phenological expression at the individual tree level [7]. Utilizing such high-resolution UAV data to analyze phenological indicators like flowering and autumn coloring, Observations repeatedly confirmed that seasonal phenomena are expressed with time lags even within the same individual. This contrasts with the implicit assumption that phenological responses occur synchronously across an entire individual, suggesting that phenology can be spatially dispersed within an individual crown [12].

This phenomenon is likely closely related to the microclimatic heterogeneity formed within the crown of the same individual. Leaves and branches constituting the crown experience different solar radiation environments depending on azimuth, slope, and occlusion, even under identical ambient air temperature conditions. These differences induce variations in physiological processes such as leaf temperature, transpiration, and photosynthetic activity [13,14]. The crown structure mediates these light and thermal environments, thereby regulating the spatial dispersion of phenological responses within the crown. This asynchrony may be particularly pronounced in species with deep or structurally complex crowns [12,15].

Generally, plant phenology is known to be controlled by cumulative temperature [16], and, accordingly, many studies have used air temperature data as a key environmental variable. However, this approach fails to sufficiently reflect microclimatic differences formed at the intra-individual or intra-crown level and has limitations in explaining the spatial heterogeneity created by crown structure. Cumulative solar duration is an indicator that reflects the cumulative effect of cumulative solar duration energy experienced by each point of the crown over a certain period [17], capable of expressing time-integrated microclimatic differences rather than environmental conditions at a single point in time. Due to these characteristics, cumulative solar duration is evaluated as a suitable variable for quantifying the spatial heterogeneity of the light environment within the crown and interpreting phenological responses from the perspective of cumulative energy [12,15,17].

Based on this perspective, this study moves beyond the existing approach of interpreting phenological responses as an average result of an individual and focuses on the microclimatic heterogeneity occurring within the same individual and the spatiotemporal dispersion of phenological responses. The high-resolution UAV-based approach provides a means to directly observe the spatial complexity within the crown and offers the potential to more precisely understand the diversity of phenological responses at the individual level in the context of increasing environmental variability and extreme weather events due to climate change.

In this context, this study aimed to investigate the effects of intra-crown microclimatic heterogeneity on the spatiotemporal patterns of phenological events, specifically flowering and autumn senescence. To isolate the 'pure' effect of canopy architecture from confounding topographic noise such as slope or aspect, the research was intentionally conducted on flat terrain. To this end, the spatial variation in cumulative solar duration within individual trees was quantified using phenological color indices extracted from time-series UAV orthomosaics and Digital Surface Models (DSMs) generated during photogrammetry.

Furthermore, the Phenological Buffering Hypothesis [18] was tested by analyzing whether the temporal duration of phenological events increases—indicating spatial asynchrony—as the microclimatic complexity (i.e., the spatial dispersion of cumulative solar duration) increases within the same individual. Additionally, the response time lag (Velocity Gap) between sunlit and shaded areas within the crown was evaluated to verify the Phenological Velocity Hypothesis [9,19], examining whether cumulative solar duration accelerates or delays the timing of flowering and autumn senescence using empirical data.

2. Materials and Methods

2.1. Study Site

This study was conducted at the Korea National Arboretum (KNA), where long-term ecological monitoring for phenology in response to climate change is underway. The KNA is located within Gwangneung Forest in Soheul-eup, Pocheon-si, Gyeonggi-do, Republic of Korea. Gwangneung Forest is designated as a UNESCO Biosphere Reserve in recognition of its high ecological conservation value.

The specific study site is the exhibition garden area within the KNA (Figure 1). This area is characterized by flat terrain, which was intentionally selected as an experimental control. Such topographical characteristics minimize confounding variables, such as rapid changes in cumulative solar duration and geometric distortion caused by slope or aspect. This setup provides optimal conditions for isolating the "pure" 3D crown structure effects and the impact of neighboring objects (e.g., adjacent trees or buildings) on intra-crown microclimatic heterogeneity by excluding complex terrain-induced noise.

2.2. Target Species

As mentioned in the introduction, the research topic was derived from phenological monitoring experiments using time-series orthomosaics. The KNA exhibition garden contains various long-term ecological monitoring plants. Plants suitable for the purpose of this study were required to have distinct phenological characteristics and fully exposed crowns in orthomosaics. Therefore, phenological phenomena were set as flowering and autumn coloring, and two species were selected: *Rhododendron yedoense* f. *poukhanense* (H.Lév.) M. Sugim (hereinafter RY) and *Acer triflorum* Kom. (hereinafter AT), both of which showed intact crowns in the orthomosaics.

RY is a semi-evergreen shrub endemic to Korea and widely distributed across the country. It blooms with vivid pink flowers from April to May. This species was selected because it has a distinct flowering period and flowering occurs across the entire crown. AT is a deciduous broad-leaved tree native to Korea and Manchuria. It exhibits uniform autumn coloring characteristics, turning from vivid orange to red in the fall, making it suitable for studying sensitivity to environmental signals such as photoperiod.

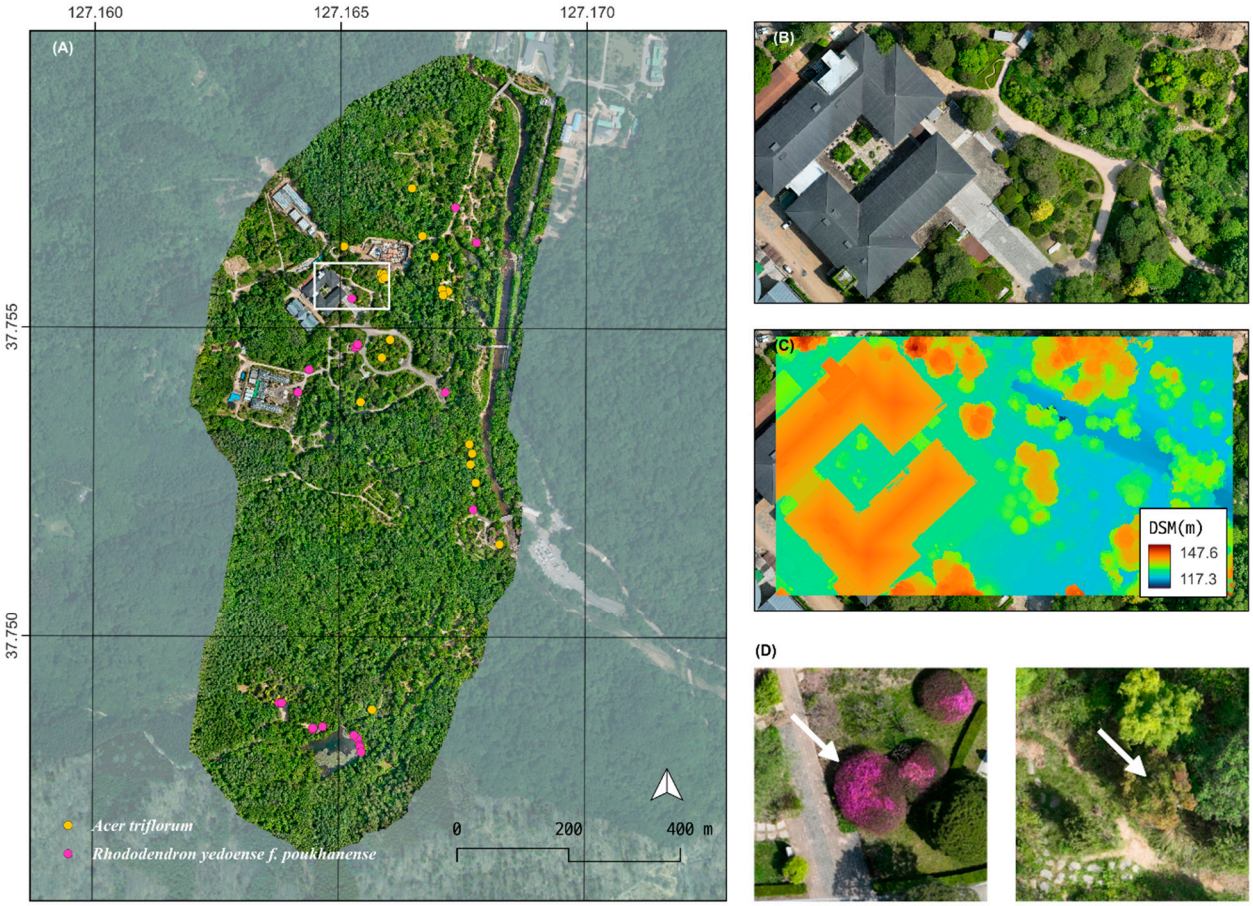


Figure 1. Study site and spatial distribution of target species. (**A**) Orthomosaic of the exhibition garden at the Korea National Arboretum (KNA). Yellow and pink dots indicate the locations of *Acer triflorum* Kom. (AT) and *Rhododendron yedoense* f. *poukhanense* (H.Lév.) M. Sugim (RY) individuals, respectively. The central white box indicates the extent of the enlarged views shown in (**B**,**C**). (**B**) Close-up view of the orthomosaic, demonstrating the high-resolution quality of the imagery used in this study. (**C**) Digital Surface Model (DSM) of the same area as (**B**), displaying elevation information derived from the 3D structure of the trees. (**D**) Close-up imagery of the target species. White arrows highlight phenological asynchrony within single individuals, showing spatially heterogeneous timing of flowering (**left**, RY) and autumn senescence (**right**, AT) across different crown sectors.

2.3. Image Acquisition and Orthomosaic Generation

High-resolution time-series imagery was acquired using a DJI Mavic 3 Multispectral (M3M) unmanned aerial vehicle (UAV; SZ DJI Technology Co., Ltd., Shenzhen, China), which served as the primary aerial platform for this study. This aircraft is equipped with a Real-Time Kinematic (RTK) module, ensuring precise positional accuracy at the centimeter level during repeated flights. Additionally, an incident light sensor mounted on the top of the aircraft performed radiometric calibration for each shooting date according to changes in sunlight intensity, securing spectral consistency of the time-series data.

Data acquisition was carried out from 11 April 2025 to 1 November 2025, with a total of 23 flights. The flight interval was flexibly adjusted according to the rate of phenological change. Specifically, during the general growing season (July–September), when phenological changes in the target plants were minimal, flights were conducted twice a month. In contrast, during major transition periods (flowering and autumn coloring), when rapid phenological events occurred, the frequency was increased to four times a month for precise capture.

The flight altitude was set to approximately 65 m above ground level (AGL), a minimum safety altitude considering obstacles such as transmission towers, and the terrain-follow mode was maintained. To ensure consistency in shadow effects, all flights were performed at 10:00 a.m., when the solar elevation is relatively stable. The flight schedule was established in compliance with safety regulations, restricting flights to once a week on days when the KNA was closed.

The acquired raw images underwent stitching and orthorectification DJI Terra software (SZ DJI Technology Co., Ltd., Shenzhen, China). The average Ground Sample Distance (GSD) of the generated orthomosaics was approximately 0.023 m.

2.4. Digital Surface Model and Cumulative Solar Duration

The Digital Surface Model (DSM) was generated during the orthomosaic processing in DJI Terra, and its initial resolution was identical to that of the orthomosaic (0.023 m). Cumulative solar duration was calculated using the r.sun.insoltime module in QGIS [20]. To ensure a time-integrated measure of the light environment, 1 January 2025, was set as DOY 1, and the cumulative solar duration (hours) was continuously accumulated from this start date up to each specific UAV flight date.

Considering both computational efficiency and the need to mitigate radiometric noise—such as wind-induced leaf flutter and transient internal shadows inherent in ultra-high-resolution imagery—the DSM was resampled to a 0.5 m resolution. This downscaling served as a spatial filter to enhance the signal-to-noise ratio for phenological event detection while maintaining a sufficient number of pixels per individual crown for robust statistical analysis.

2.5. Data Extraction for Target Plants

To extract the RGB signals and cumulative solar duration of the target plants, crown polygons were manually delineated for individuals by meticulously comparing the entire time-series orthomosaics to ensure the crowns were fully visible and healthy throughout the study period.

A total of 20 individuals per species were selected; this sample size was determined by the maximum number of *A. triflorum* (AT) individuals that met our strict inclusion criteria of having completely exposed crowns without occlusion from neighboring tall trees. Although more candidates were available for *R. yedoense* f. *poukhanense* (RY), the sample size was matched to 20 to maintain a balanced comparative design between the two species. To ensure statistical and spatial independence, the selected individuals were verified to have no mutual shading interactions or crown overlaps. To spatially decompose minute phenological changes within individual trees and to filter radiometric noise (e.g., transient shadows, wind-induced leaf movement) inherent in high-resolution orthomosaics, the individual polygons were divided into 0.5 m grids identical to the resampled DSM.

This resolution served as a spatial filter to improve the signal-to-noise ratio for phenological event detection while retaining sufficient grid cells per crown for robust statistical analysis. The RGB Digital Numbers (DN) and cumulative solar duration from the time-series orthomosaics were extracted for each grid and returned as an integrated time-series dataframe.

For each grid i, normalized chromatic coordinates specialized for RGB bands were calculated [21]. Specifically, the Red Chromatic Coordinate (RCC) was used for flowering detection in RY, and the Green Chromatic Coordinate (GCC) was used for autumn senescence detection in AT (Equation (1)).

$$RCC_i = \frac{R_i}{R_i + G_i + B_i}, GCC_i = \frac{G_i}{R_i + G_i + B_i} \quad (1)$$

2.6. Phenological Event Detection Using Derivatives

To remove noise from the time-series data and extract precise dates of phenological events, smoothing spline and derivative analysis methods were applied [22]. A smoothing function $f(t)$ was fitted to the time-series data $y(t)$ of each grid. To prevent overfitting, the smoothing parameter ($Spar$) was set to 0.4–0.5. The event date (D_{event}) was defined as the point where the first derivative $f'(t)$ of the fitted function reached a local extremum, representing the point of maximum rate of change in vegetation color.

The selection of indices and extrema followed established protocols from prior phenological research [23] to ensure optimal sensitivity for each species: the local maximum of the Red Chromatic Coordinate (RCC) derivative was utilized for RY to capture the rapid onset of pink flowering, while the local minimum of the Green Chromatic Coordinate (GCC) derivative was applied for AT to detect the sharp decline in chlorophyll during senescence onset. The calculation for D_{event} is defined as follows (Equation (2)):

$$D_{event} = \begin{cases} \underset{t\in[100,\ 150]}{\text{argmax}}\ f'_{RCC}(t) & for\ Spring\ (Flowering\ of\ RY) \\ \underset{t\in[250,\ 300]}{\text{argmin}}\ f'_{GCC}(t) & for\ Autumn\ (Senescence\ of\ AT) \end{cases} \quad (2)$$

To prevent false positives caused by radiometric noise or secondary growth, the search window was restricted to DOY 100–150 for RY and DOY 250–300 for AT. These windows were established based on long-term ecological monitoring baseline data from the KNA, which define the typical phenological windows for these target species at the study site.

2.7. Statistical Analysis: Buffering and Velocity Hypotheses

To investigate the effect of intra-crown microclimatic heterogeneity on phenology, the data were aggregated from the grid level to the individual level, and two hypotheses were tested.

First, to test the Phenological Buffering Hypothesis, a linear regression analysis was performed between the standard deviation of cumulative solar duration ($SD_{solar,\,k}$) and the standard deviation of event dates ($SD_{pheno,\,k}$) within each individual k (Equation (3)).

Prior to the regression analysis, the fundamental assumptions of linear modeling—including the normality and homoscedasticity of residuals—were verified to ensure the validity of the statistical inferences.

$$SD_{pheno,k} = \beta_0 + \beta_1 \cdot SD_{solar,k} + \epsilon_k \quad (3)$$

Here, if $\beta_1 > 0$, it is interpreted as supporting a bet-hedging strategy where phenological duration increases as the microclimate becomes more complex [24].

Second, to test the Phenological Velocity Hypothesis, the mean difference (Gap) in reaction dates between the top 20% (sunlit) and bottom 20% (shaded) grids for cumulative solar duration within each individual was calculated (Equation (4)).

$$G_{ap_k} = \begin{cases} \overline{D}_{shaded} - \overline{D}_{sunlit} & (Spring:\ RY) \\ \overline{D}_{sunlit} - \overline{D}_{shaded} & (Autumn:\ AT) \end{cases} \quad (4)$$

A positive value ($G_{ap_k} > 0$) consistently indicates that sunlit areas act to extend the growing season relative to shaded areas (i.e., earlier flowering in spring or later senescence in autumn).

https://doi.org/10.3390/f17030342

2.8. Software and Packages

Time-series orthomosaic processing was performed using DJI Terra software [25], and cumulative solar duration calculation used the r.sun.insoltime module in QGIS [24]. All subsequent spatial data processing and statistical analyses were conducted in the R software environment [26]. Large-scale raster and vector data processing utilized the terra [27] and sf [28] packages. Time-series preprocessing and manipulation were handled using dplyr and tidyr [29], while statistical hypothesis testing and visualization were performed using stats, ggplot2, and ggtext [30]. All R packages used for spatial data processing and statistical analysis were accessed via their respective official CRAN or developer repositories as cited, and their specific version information and source code are available through the provided references.

Additionally, Google Gemini (Google LLC, Mountain View, CA, USA) was utilized to generate the schematic illustration of the research workflow (Figure 2) and to refine the R [26] script logic for data visualization.

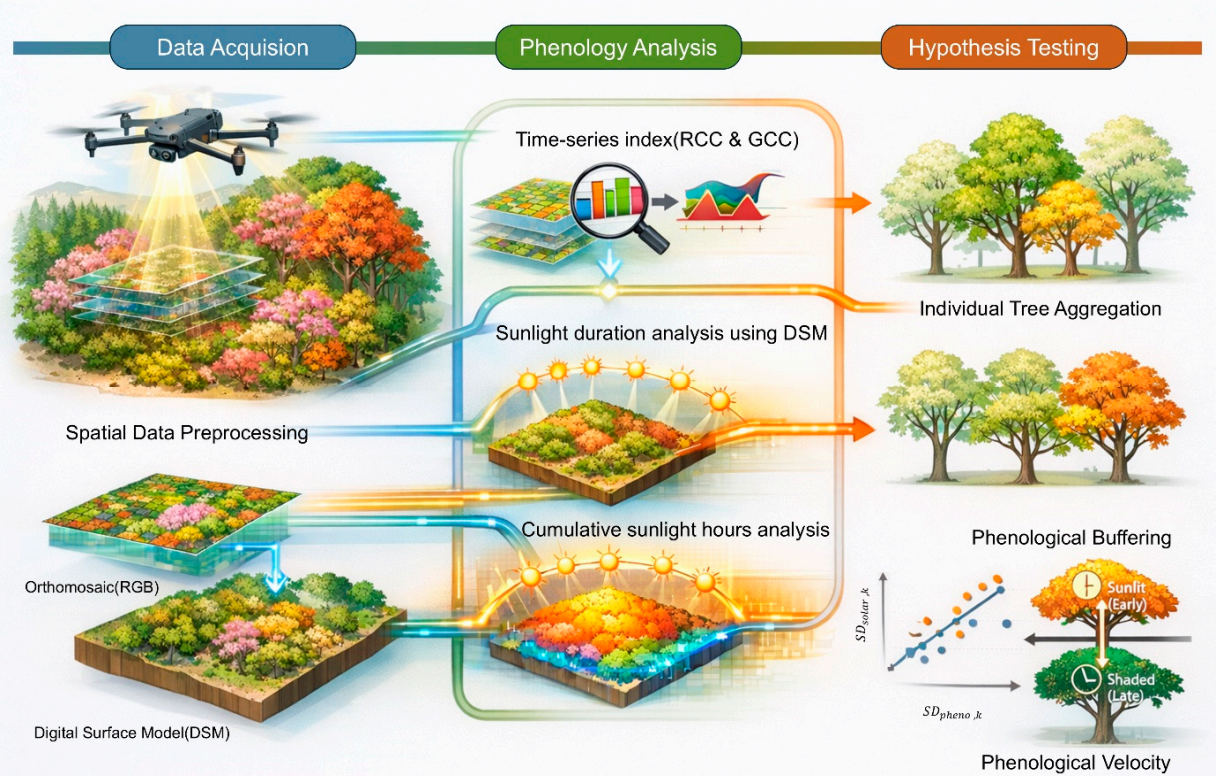


Figure 2. Overall workflow of the research methodology applied in this study. The research process consists of three main stages: (1) Data Acquisition and Preprocessing: Acquiring UAV imagery and processing it into orthomosaics and Digital Surface Models (DSMs); (2) Data Extraction: Deriving grid-level phenological dates using derivative analysis and generating microclimatic variables through solar duration modeling; and (3) Statistical Analysis: Aggregating data to the individual-tree level to test the Phenological Buffering and Velocity Hypotheses.

2.9. Use of Generative AI Tools

During the preparation of this manuscript, the authors used two Generative AI tools under the authors' supervision. First, Google Gemini (Google LLC: Mountain View, CA, USA) was used to assist in drafting R code structures and expressing mathematical formulations based on the authors' original analytical logic; however, all statistical models, computational procedures, and analytical frameworks were entirely conceived, designed, and validated by the authors. Second, ChatGPT (OpenAI, San Francisco, CA, USA) was

used solely to generate an initial schematic layout for Figure 2, while all scientific content, labeling, and final graphical composition were authored and edited by the authors. Finally, Google Gemini was also used for minor English polishing to improve sentence clarity and readability.

No AI tools were used for data generation, processing, statistical analysis, phenological event detection, or interpretation of scientific results. All AI-assisted outputs were thoroughly reviewed, verified, and edited by the authors, who take full responsibility for the content of this publication.

3. Results

3.1. Phenological Event Detection via Time-Series Derivative Analysis

In this study, smoothing splines and derivative analysis were applied to UAV-based high-resolution time-series vegetation indices (RCC, GCC) to detect phenological events at the 0.5 m grid unit within individual trees. Figure 3 shows representative examples where this detection algorithm was applied.

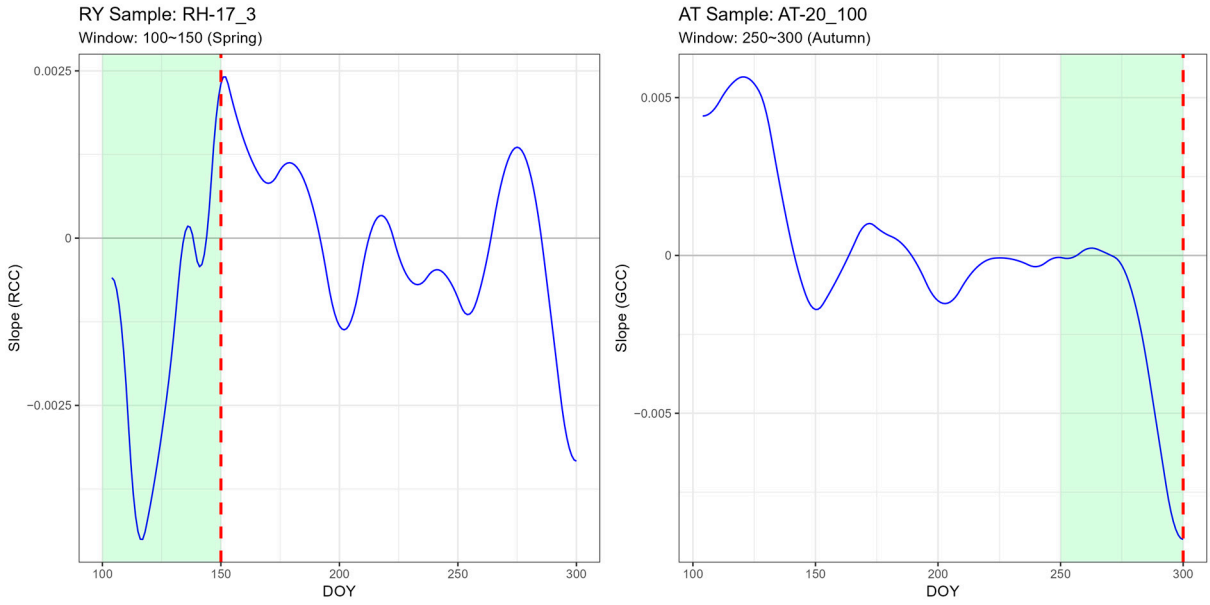


Figure 3. Representative examples of phenological event detection using derivative analysis of UAV-based time-series vegetation indices. (**Left**) Detection of flowering onset for RY. The event date was defined as the point of maximum rate of change (local maximum of the first derivative) in the Red Chromatic Coordinate (RCC) within the spring search window (DOY 100–150, shaded green). (**Right**) Detection of senescence onset for AT. The event date was identified as the point of minimum rate of change (local minimum) in the Green Chromatic Coordinate (GCC) within the autumn search window (DOY 250–300). The red dashed lines indicate the determined event dates.

The statistical results of phenological events calculated by applying this algorithm to all trees are presented in Table 1. For RY, valid flowering events were detected in a total of 4213 grids, with a mean flowering date of DOY 122.9 (±1.46). Flowering timing ranged from DOY 118 to 127, confirming that the detected events were concentrated within a relatively narrow period.

For AT, senescence events were detected in a total of 2674 grids. The mean senescence date was DOY 294.5 (±1.57), with a range from DOY 290 to 299. In both species, the standard deviation of the phenological event timing was approximately 1.5 days, demonstrating that the approach based on UAV imagery and the rate of change in vegetation indices could stably detect phenological event timings even within the crowns of individual trees.

Table 1. Summary statistics of phenological event dates (DOY) and cumulative solar duration derived from UAV imagery. The event dates were determined based on the peak derivative of vegetation indices as illustrated in Figure 3.

Species	Phenological Event	N_{grid}	Event Date (DOY)			Solar Duration
			Mean	SD	Range (Min–Max)	Mean (h)
R. yedoense f. *poukhanense*	Spring Flowering	4213	122.9	1.46	118–127	258.4
A. triflorum	Autumn Senescence	2674	294.5	1.57	290–299	1412.8

Note: N_{grid} refers to the total number of 0.5 m × 0.5 m grid cells where phenological events were successfully detected. DOY denotes Day of Year. SD denotes Standard Deviation.

3.2. Species Differences in Phenological Responses to Intra-Crown Light Heterogeneity

Based on the confirmation in Section 3.1 that phenological event timings could be stably detected at the 0.5 m grid level, the analysis examined how the distribution of cumulative solar duration within the crown affected the spatial dispersion of phenological events and the response time lag by sector (Figure 4, Table 2).

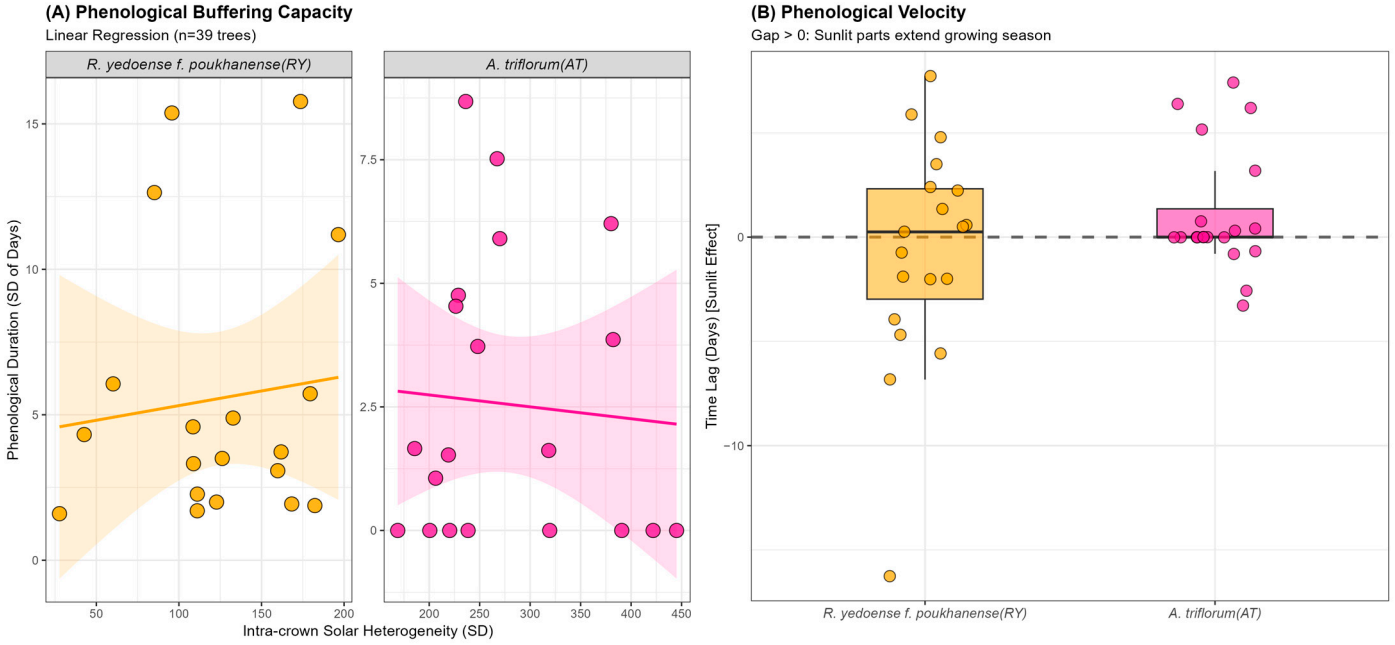


Figure 4. Species-specific relationships between intra-crown microclimatic heterogeneity and phenological responses. (**A**) Relationships between intra-crown variability in cumulative solar radiation (SD_{Solar}) and phenological event duration (SD_{Pheno}) at the individual-tree level. Each point represents a single tree. Solid lines indicate species-specific linear trends, illustrating contrasting responses of phenological duration to increasing microclimatic heterogeneity. (**B**) Species-level differences in phenological velocity, expressed as the timing difference between sunlit and shaded crown sectors (Velocity Gap = Sunlit − Shaded). Boxplots show the distribution of velocity gaps for each species, with points representing individual trees. The dashed horizontal line indicates zero difference.

The analysis of the relationship between intra-crown light environment heterogeneity and phenological event duration revealed contrasting, though statistically weak, response patterns between the two species (Figure 4A).

For RY, the duration of phenological events showed a slight positive association with the variability of cumulative solar duration (R^2 = 0.011), yet this relationship was not statistically significant (ρ = 0.668). This suggests that while microclimatic complexity might contribute to spatial asynchrony in flowering, other physiological factors likely buffer the canopy against light-induced dispersion.

Table 2. Species-level summary of intra-crown microclimatic heterogeneity, phenological response metrics, and linear regression model diagnostics derived from UAV imagery.

Species	N_{tree}	Mean N_{cells}	SD_{Solar}	SD_{Pheno}	Velocity Gap	R^2	ρ-Value	ρBP	ρSW
A. triflorum	20	132.2	278.7 ± 83.9	2.55 ± 2.86	+1.12 ± 2.95	0.005	0.767	0.798	0.00
R. yedoense f. *poukhanense*	19	29.8	123.9 ± 48.3	5.56 ± 4.63	−0.77 ± 5.39	0.011	0.668	0.700	0.00

N_{tree} number of individual trees analyzed. N_{cells} average number of 0.5 m resolution grid cells per individual crown. SD_{Solar} & SD_{Pheno} Standard Deviation of intra-crown solar duration variability and phenological event duration across individuals. Velocity Gap mean difference in phenological timing between sunlit and shaded sectors (Positive values indicate extended growing season in sunlit areas). ρBP denotes the ρ-value from the Breusch–Pagan test for homoscedasticity. ρSW denotes the ρ-value from the Shapiro–Wilk tes for homoscedasticity.

Conversely, in AT, the duration of phenological events showed a negligible negative trend with increasing solar heterogeneity (R^2 = 0.005, ρ = 0.767). To ensure the statistical validity of these observations, diagnostic tests were performed on the regression models. Both species satisfied the assumption of homoscedasticity ($\rho BP > 0.7$), indicating stable variance in phenological responses. However, the normality test for residuals indicated deviations ($\rho SW < 0.01$), reflecting the high individual-level variability inherent in natural forest populations (Table 2).

This interspecific difference was further examined through the Velocity Gap analysis, which represents the phenological response time lag by crown sector (Figure 4B).

In AT, the phenological transition in sunlit sectors occurred later than in shaded sectors on average (Mean Gap = +1.12 ± 2.95 days). Although this trend did not reach statistical significance (ρ = 0.105), the positive directionality aligns with the hypothesis that sunlit areas extend the growing season (i.e., delayed senescence).

In contrast, RY exhibited a slightly negative and highly variable velocity gap (Mean Gap = −0.77 ± 5.39 days; ρ = 0.540). The lack of a significant directional lag suggests that flowering onset in this shrub species is not strictly governed by direct light exposure, further supporting the presence of a strong internal buffering mechanism that maintains whole-crown synchrony despite external light gradients.

In summary, while RY showed a potential tendency for phenological responses to be spatially dispersed as intra-crown light environment heterogeneity increased, AT demonstrated a robust pattern where phenological transition timings remained relatively synchronous at the individual level, effectively buffering against high environmental heterogeneity.

4. Discussion

4.1. Ecological Significance of Intra-Individual Phenological Asynchrony and Buffering Effects

The results of this study suggest the need to re-examine the implicit assumption that phenological responses occur synchronously across an entire individual. Existing satellite-based phenology studies have mainly analyzed phenology based on average signals at the regional or community scale, often treating individual trees as single points or homogeneous pixels [5].

However, using high-resolution UAV imagery, it was confirmed that the timing of phenological events such as flowering and autumn coloring varies depending on the spatial units constituting the crown, even within the same individual. Although the linear correlation between microclimatic heterogeneity and phenological dispersion was statistically weak ($R^2 < 0.02$, $\rho > 0.05$), this very lack of a strong linear dependency implies that phenological buffering is not realized through a simple passive response to light conditions, but through complex asynchronous responses within the individual's space [22,31,32]. That is, even in the same tree, phenological transition starts earlier in some parts of the crown, while it proceeds relatively later in others. This spatial dispersion acts to moderate the

phenological response observed at the individual level. This can be interpreted as adding a spatial dimension to the existing perspective that explained phenological buffering only in terms of changes along the time axis [6].

In particular, the intra-individual phenological asynchrony confirmed in this study was related to intra-crown microclimatic heterogeneity, albeit non-linearly. Cumulative solar duration varied spatially depending on crown structure, branch arrangement, azimuth, and occlusion conditions, and these differences in energy input provided the environmental context for the spatial dispersion of phenological response timings. The fact that high solar heterogeneity did not lead to excessive phenological dispersion demonstrates that phenological responses are not uniformly controlled by a single external climate signal but are regulated by a combination of minute environmental conditions and internal physiological integration experienced within the individual [33,34].

From this perspective, phenological buffering can be understood as an emergent property of how an individual responds to environmental fluctuations [19,35]. In other words, even as intra-individual microclimatic heterogeneity increases, the average phenological response of the entire individual remains robust, suggesting that the plant is actively buffering against rapid environmental changes. This provides important implications for explaining how phenological stability at the individual level can be maintained under environmental conditions where climate variability is increasing.

4.2. Species Differences in Phenological Responses by Crown Structure and Growth Form

In this study, phenological response patterns to intra-crown light environment heterogeneity appeared contradictory depending on the species, supported by the Velocity Gap analysis. RY, a shrub species, exhibited a negative velocity gap (Mean Gap ≈ -0.8 days), suggesting that flowering onset is not strictly coupled with direct light exposure. In contrast, AT, a tree species, showed a positive velocity gap (Mean Gap $\approx +1.1$ days), indicating a trend where sunlit sectors extend the growing season, although this maintained relative synchrony at the individual level even under conditions of high-light environment heterogeneity.

These differences are likely related to differences in how the environment is experienced within the individual according to crown structure and growth form, rather than simple differences in environmental response [12,15,36].

RY is a shrub species with relatively low height and simple crown structure, where the contrast in light environment within the crown is formed relatively gently. Under these structural characteristics, the non-significant relationship between solar heterogeneity and phenological duration suggests that internal factors likely override microclimatic signals, preventing excessive spatial dispersion of flowering timings [12,35,37,38]. The slight increase in phenological duration variability observed in RY can be interpreted as a limited response to these spatial dispersion effects.

On the other hand, AT is a tree species with great height and complex branch arrangement and crown shape, forming very large light environment heterogeneity within the crown. Nevertheless, a tendency for the duration of phenological events to decrease or remain stable as light environment heterogeneity increased was observed in AT ($\rho = 0.767$). This suggests that microclimatic differences within the crown are not directly linked to spatial dispersion of phenological responses, and that strong regulation operates to maintain the timing of phenological transition within a narrow period at the individual level.

These interspecific differences imply the possibility that phenological responses are not determined independently at the individual leaf or branch unit but are integrated by the physiological state and structural constraints of the entire individual. Particularly in tree species, even if phenological transition is delayed or accelerated in some parts of the crown,

the timing of leaf fall or dormancy transition for the entire individual may be restricted so as not to be dispersed beyond a certain level [12]. This is because excessive asynchrony of phenological responses in species with large crown scales can act disadvantageously to the individual's seasonal transition efficiency or survival strategy [15,39,40].

4.3. Ecological Validity of the Cumulative Solar Duration Approach

This study used cumulative solar duration on the crown surface as a variable for phenological response. Generally, plant phenological expression is known to be controlled by cumulative temperature, and consequently, many phenological studies have utilized air temperature data as a key environmental variable [16]. However, this approach has limitations in reflecting microclimatic differences at the intra-individual or intra-crown level [12] and finds it difficult to sufficiently explain the spatial heterogeneity formed by crown structure.

Cumulative solar duration is an indicator reflecting the accumulation of solar radiation energy per unit time, capable of directly expressing spatial differences in solar duration within the crown [17]. Leaves and branches constituting the crown receive different solar radiation conditions depending on azimuth, slope, and occlusion even under the same ambient air temperature conditions, and these differences affect physiological processes such as leaf temperature, transpiration, and photosynthetic activity [41,42]. Therefore, cumulative solar duration can be understood not as an alternative indicator independent of air temperature, but as a variable that integrally reflects the energy environment resulting from the combination of crown structure and microclimatic conditions.

In particular, this study calculated cumulative solar duration considering the spatial shape of the 3D crown surface by combining UAV-based orthomosaics and DSMs generated during the photogrammetry process. This approach has the advantage of directly reflecting the crown structure and occlusion effects of individual trees, unlike solar radiation data at the surface or weather station level. As a result, a distinct distribution of cumulative solar duration was formed for each crown part even within the same individual, which provided the basis for analyzing the spatial dispersion of phenological events.

Furthermore, cumulative solar duration is a suitable variable for phenological research in that it allows phenological responses to be interpreted as a cumulative effect over a certain period rather than environmental conditions at a single point in time [43]. Phenological events are often induced gradually by the cumulative effects of energy and temperature rather than determined by the momentary arrival of specific threshold conditions [19,44]. From this perspective, cumulative solar duration acts as an ecologically meaningful indicator in explaining the timing and speed of phenological responses.

4.4. Methodological Limitations and Expandability

Although this study analyzed the spatial patterns of intra-individual phenological responses by combining high-resolution UAV imagery and 3D crown structure information, it has several methodological limitations.

First, this study was an analysis performed in a single region and a single year, and the low statistical significance ($\rho > 0.05$) observed in our regression models may be partly attributed to this temporal limitation. Additional verification is needed to determine whether the observed relationship between phenological response and microclimatic heterogeneity appears identically under other climate conditions or in other years. Second, this study used cumulative solar duration as the main explanatory variable for phenological response and did not directly consider other environmental factors such as temperature, moisture status, and soil conditions. Therefore, it is reasonable to interpret the results of this study as showing that intra-crown microclimatic heterogeneity is one of the contributing fac-

tors, rather than explaining phenological responses by a single factor. Third, since the target species were limited to one tree species and one shrub species, caution is needed in generalizing the interspecific differences observed in this study.

Nevertheless, the methodology of this study has significant meaning in that it presents a new analytical framework capable of quantitatively analyzing intra-individual phenological responses. The approach combining UAV-based ultra-high-resolution imagery and DSMs generated by photogrammetry allows for the simultaneous consideration of intra-crown spatial structure and microclimatic heterogeneity, which were difficult to access with existing satellite imagery or ground observations.

5. Conclusions

This study quantitatively identified the heterogeneity of phenological responses at the intra-individual crown level, which has been overlooked in existing remote sensing-based phenological research, by combining high-resolution UAV time-series imagery and 3D crown structure information.

The analysis results showed that the timing of flowering and autumn coloring appeared differently depending on the spatial units constituting the crown even within the same individual. While the linear relationship between this asynchrony and intra-crown microclimatic heterogeneity was not statistically strong ($R^2 < 0.02$), the findings suggest a robust buffering mechanism. In particular, phenological responses to intra-crown light environment heterogeneity appeared in different patterns depending on the species; in the shrub species (RY), the spatial dispersion of phenological responses was independent of direct light exposure, whereas in the tree species (AT), synchrony at the individual level tended to be relatively maintained despite high light heterogeneity.

These findings suggest that phenological buffering is not a single mechanism but can be implemented differently depending on crown structure and growth form. This study presents a new analytical perspective that considers intra-individual spatial structure and microclimatic conditions, moving beyond the existing approach that interpreted phenological responses as the average signal of the entire individual. This approach will provide important fundamental data for understanding how plant individuals regulate and maintain phenological responses in situations where environmental variability increases due to climate change.

Author Contributions: Conceptualization, D.-H.K.; methodology, M.-K.P. and D.-H.K.; software, M.-K.P.; validation, M.-K.P., Y.-Y.K. and H.-G.C.; formal analysis, M.-K.P.; investigation (UAV data acquisition and processing), M.-K.P.; investigation (phenological field observations and site management), Y.-Y.K. and H.-G.C.; data curation, M.-K.P.; writing—original draft preparation, M.-K.P.; writing—review and editing, M.-K.P. and D.-H.K.; visualization, M.-K.P.; supervision, D.-H.K.; project administration, D.-H.K.; funding acquisition, D.-H.K. All authors have read and agreed to the published version of the manuscript.

Funding: This study was supported by the Korea National Arboretum (KNA1-2-47-24-1).

Data Availability Statement: The source data extracted from UAV imagery (including grid-level vegetation indices and solar duration) and the complete R scripts used for the statistical analysis are openly available in Zenodo at [10.5281/zenodo.18239708]. The raw high-resolution UAV orthomosaics presented in this study are not publicly available due to copyright restrictions and large file size limitations but are available from the corresponding author upon reasonable request.

Acknowledgments: During the preparation of this work, the authors used Google Gemini (Google LLC: Mountain View, CA, USA) for the purpose of generating the schematic illustration presented in Figure 2, as well as for improving the readability and language quality of the manuscript and refining the R script logic for statistical visualization. After using this tool, the authors reviewed and edited the content as needed and take full responsibility for the content of the publication.

Conflicts of Interest: The authors declare no conflicts of interest. The funders had no role in the design of the study; in the collection, analyses, or interpretation of data; in the writing of the manuscript; or in the decision to publish the results.

References

1. Piao, S.; Liu, Q.; Chen, A.; Janssens, I.A.; Fu, Y.; Dai, J.; Liu, L.; Lian, X.; Shen, M.; Zhu, X. Plant phenology and global climate change: Current progresses and challenges. *Glob. Change Biol.* **2019**, *25*, 1922–1940. [CrossRef]
2. Legg, S. IPCC, 2021: Climate Change 2021: The Physical Science Basis. *Interaction* **2021**, *49*, 44–45.
3. Menzel, A.; Sparks, T.H.; Estrella, N.; Koch, E.; Aasa, A.; Ahas, R.; Alm-Kübler, K.; Bissolli, P.; Braslavská, O.; Briede, A.; et al. European phenological response to climate change matches the warming pattern. *Glob. Change Biol.* **2006**, *12*, 1969–1976. [CrossRef]
4. Thackeray, S.J.; Henrys, P.A.; Hemming, D.; Bell, J.R.; Botham, M.S.; Burthe, S.; Helaouet, P.; Johns, D.G.; Jones, I.D.; Leech, D.I. Phenological sensitivity to climate across taxa and trophic levels. *Nature* **2016**, *535*, 241–245. [CrossRef] [PubMed]
5. White, M.A.; De Beurs, K.M.; Didan, K.; Inouye, D.W.; Richardson, A.D.; Jensen, O.P.; O'Keefe, J.; Zhang, G.; Nemani, R.R.; Van Leeuwen, W.J.D.; et al. Intercomparison, interpretation, and assessment of spring phenology in North America estimated from remote sensing for 1982–2006. *Glob. Change Biol.* **2009**, *15*, 2335–2359. [CrossRef]
6. Dronova, I.; Taddeo, S. Remote sensing of phenology: Towards the comprehensive indicators of plant community dynamics from species to regional scales. *J. Ecol.* **2022**, *110*, 1460–1484. [CrossRef]
7. Richardson, A.D.; Hufkens, K.; Milliman, T.; Frolking, S. Intercomparison of phenological transition dates derived from the PhenoCam Dataset V1. 0 and MODIS satellite remote sensing. *Sci. Rep.* **2018**, *8*, 5679. [CrossRef]
8. Zhang, X.; Friedl, M.A.; Schaaf, C.B.; Strahler, A.H.; Hodges, J.C.; Gao, F.; Reed, B.C.; Huete, A. Monitoring vegetation phenology using MODIS. *Remote Sens. Environ.* **2003**, *84*, 471–475. [CrossRef]
9. Richardson, A.D.; Keenan, T.F.; Migliavacca, M.; Ryu, Y.; Sonnentag, O.; Toomey, M. Climate change, phenology, and phenological control of vegetation feedbacks to the climate system. *Agric. For. Meteorol.* **2013**, *169*, 156–173. [CrossRef]
10. Tanner, R.L.; Dowd, W.W. Inter-individual physiological variation in responses to environmental variation and environmental change: Integrating across traits and time. *Comp. Biochem. Physiol. Part A Mol. Integr. Physiol.* **2019**, *238*, 110577. [CrossRef]
11. Yao, H.; Qin, R.; Chen, X. Unmanned aerial vehicle for remote sensing applications—A review. *Remote Sens.* **2019**, *11*, 1443. [CrossRef]
12. Zahnd, C.; Arend, M.; Kahmen, A.; Hoch, G. Microclimatic gradients cause phenological variations within temperate tree canopies in autumn but not in spring. *Agric. For. Meteorol.* **2023**, *331*, 109340. [CrossRef]
13. Lorer, E.; Verheyen, K.; Blondeel, H.; De Pauw, K.; Sanczuk, P.; De Frenne, P.; Landuyt, D. Forest understorey flowering phenology responses to experimental warming and illumination. *New Phytol.* **2023**, *241*, 1476–1491. [CrossRef]
14. Fauset, S.; Freitas, H.C.; Galbraith, D.R.; Sullivan, M.J.P.; Aidar, M.P.M.; Joly, C.A.; Phillips, O.L.; Vieira, S.A.; Gloor, M.U. Differences in leaf thermoregulation and water use strategies between three co-occurring Atlantic forest tree species. *Plant Cell Environ.* **2018**, *41*, 1618–1631. [CrossRef]
15. Wu, X.; Niu, C.; Liu, X.; Hu, T.; Feng, Y.; Zhao, Y.; Liu, S.; Liu, Z.; Dai, G.; Zhang, Y. Canopy structure regulates autumn phenology by mediating the microclimate in temperate forests. *Nat. Clim. Change* **2024**, *14*, 1299–1305. [CrossRef]
16. Chuine, I.; Régnière, J. Process-Based Models of Phenology for Plants and Animals. *Annu. Rev. Ecol. Evol. Syst.* **2017**, *48*, 159–182. [CrossRef]
17. Hofierka, J.; Suri, M. The solar radiation model for Open source GIS: Implementation and applications. In Proceedings of the Open Source GIS-GRASS Users Conference, Trento, Italy, 11–13 September 2002.
18. De Frenne, P.; Rodríguez-Sánchez, F.; Coomes, D.A.; Baeten, L.; Verstraeten, G.; Vellend, M.; Bern-hardt-Römermann, M.; Brown, C.D.; Brunet, J.; Cornelis, J.; et al. Microclimate moderates plant responses to macroclimate warming. *Proc. Natl. Acad. Sci. USA* **2013**, *110*, 18561–18565. [CrossRef] [PubMed]
19. Chuine, I. A unified model for budburst of trees. *J. Theor. Biol.* **2000**, *207*, 337–347. [CrossRef] [PubMed]
20. QGIS Development Team. QGIS Geographic Information System, Version 3.34. 2025. Available online: https://www.qgis.org (accessed on 14 October 2025).
21. Sonnentag, O.; Hufkens, K.; Teshera-Sterne, C.; Young, A.M.; Friedl, M.; Braswell, B.H.; Milliman, T.; O'Keefe, J.; Richardson, A.D. Digital repeat photography for phenological research in forest ecosystems. *Agric. For. Meteorol.* **2012**, *152*, 159–177. [CrossRef]
22. Klosterman, S.T.; Hufkens, K.; Gray, J.M.; Melaas, E.; Sonnentag, O.; Lavine, I.; Mitchell, L.; Norman, R.; Friedl, M.A.; Richardson, A.D. Evaluating remote sensing of deciduous forest phenology at multiple spatial scales using PhenoCam imagery. *Biogeosciences* **2014**, *11*, 4305–4320. [CrossRef]
23. Park, M.-K.; Kim, Y.-Y.; Choi, H.-G.; Kim, D.-H. Feasibility of Detecting Plant Phenological Events Using Time-Series UAV Orthomosaics and Color-Based Z-Scores. *Forests* **2026**, *17*, 196. [CrossRef]

24. Gallinat, A.S.; Primack, R.B.; Wagner, D.L. Autumn phenology: The neglected season. *Trends Ecol. Evol.* **2015**, *30*, 169–176. [CrossRef]
25. DJI Enterprise. DJI Terra: UAV Photogrammetry and Mapping Software, Version 5.0.0. 2025. Available online: https://enterprise.dji.com/dji-terra (accessed on 14 October 2025).
26. R Core Team. R: A Language and Environment for Statistical Computing, Version 4.5.2. 2025. Available online: https://www.R-project.org (accessed on 24 October 2025).
27. Hijmans, R.J.; Barbosa, M.; Brown, A. Terra: Spatial Data Analysis. 2026. Available online: https://rspatial.r-universe.dev/terra (accessed on 14 October 2025).
28. Pebesma, E.; Bivand, R. *Spatial Data Science: With Applications in R*; Chapman and Hall/CRC: Boca Raton, FL, USA, 2023.
29. Wickham, H.; François, R.; Henry, L.; Müller, K.; Vaughan, D. *dplyr: A Grammar of Data Manipulation*. 2023. Available online: https://CRAN.R-project.org/package=dplyr (accessed on 9 January 2026).
30. Wickham, H. *ggplot2: Elegant Graphics for Data Analysis*; Springer: New York, NY, USA, 2016.
31. Richardson, A.D.; Jenkins, J.P.; Braswell, B.H.; Hollinger, D.Y.; Ollinger, S.V.; Smith, M.-L. Use of digital webcam images to track spring green-up in a deciduous broadleaf forest. *Oecologia* **2007**, *152*, 323–334. [CrossRef]
32. Niinemets, Ü.; Valladares, F. Tolerance to shade, drought, and waterlogging of temperate northern hemi-sphere trees and shrubs. *Ecol. Monogr.* **2006**, *76*, 521–547. [CrossRef]
33. Stiegel, S.; Entling, M.H.; Mantilla-Contreras, J. Reading the leaves' palm: Leaf traits and herbivory along the microclimatic gradient of forest layers. *PLoS ONE* **2017**, *12*, e0169741. [CrossRef]
34. Bernaschini, M.L.; Trumper, E.; Valladares, G.; Salvo, A. Are all edges equal? Microclimatic conditions, geo-graphical orientation and biological implications in a fragmented forest. *Agric. Ecosyst. Environ.* **2019**, *280*, 142–151. [CrossRef]
35. Wang, Y.; Yang, X.-D.; Ali, A.; Lv, G.-H.; Long, Y.-X.; Wang, Y.-Y.; Ma, Y.-G.; Xu, C.-C. Flowering phenology shifts in response to functional traits, growth form, and phylogeny of woody species in a desert area. *Front. Plant Sci.* **2020**, *11*, 536. [CrossRef]
36. Nateshkumar, A.; Indhumathi, K.; Arunkumar, R.; Chitra, R.; Sangeetha, M.; Hariraj, N. Impact of canopy architecture on phenology and production efficiency of flower crops: A review. *Plant Sci. Today* **2025**, *12*, 10508. [CrossRef]
37. Dahlgren, J.P.; Von Zeipel, H.; Ehrlén, J. Variation in vegetative and flowering phenology in a forest herb caused by environmental heterogeneity. *Am. J. Bot.* **2007**, *94*, 1570–1576. [CrossRef]
38. Xiong, X.; Wu, H.; Wei, X.; Jiang, M. Contrasting temperature and light sensitivities of spring leaf phenology between understory shrubs and canopy trees: Implications for phenological escape. *Agric. For. Meteorol.* **2024**, *355*, 110144. [CrossRef]
39. Mariën, B.; Dox, I.; De Boeck, H.J.; Willems, P.; Leys, S.; Papadimitriou, D.; Campioli, M. Does drought advance the onset of autumn leaf senescence in temperate deciduous forest trees? *Biogeosciences* **2021**, *18*, 3309–3330. [CrossRef]
40. Yumoto, G.; Nishio, H.; Muranaka, T.; Sugisaka, J.; Honjo, M.N.; Kudoh, H. Seasonal switching of integrated leaf senescence controls in an evergreen perennial Arabidopsis. *Nat. Commun.* **2024**, *15*, 4719. [CrossRef] [PubMed]
41. Valladares, F.; Niinemets, Ü. Shade Tolerance, a Key Plant Feature of Complex Nature and Consequences. *Annu. Rev. Ecol. Evol. Syst.* **2008**, *39*, 237–257. [CrossRef]
42. Leigh, A.; Sevanto, S.; Ball, M.C.; Close, J.D.; Ellsworth, D.S.; Knight, C.A.; Nicotra, A.B.; Vogel, S. Do thick leaves avoid thermal damage in critically low wind speeds? *New Phytol.* **2012**, *194*, 477–487. [CrossRef]
43. Körner, C.; Basler, D. Phenology Under Global Warming. *Science* **2010**, *327*, 1461–1462. [CrossRef]
44. Gauzere, J.; Delzon, S.; Davi, H.; Bonhomme, M.; de Cortazar-Atauri, I.G.; Chuine, I. Integrating interactive effects of chilling and photoperiod in phenological process-based models. A case study with two European tree species: Fagus sylvatica and *Quercus petraea*. *Agric. For. Meteorol.* **2017**, *244*, 9–20. [CrossRef]

Disclaimer/Publisher's Note: The statements, opinions and data contained in all publications are solely those of the individual author(s) and contributor(s) and not of MDPI and/or the editor(s). MDPI and/or the editor(s) disclaim responsibility for any injury to people or property resulting from any ideas, methods, instructions or products referred to in the content.